International Journal of Heat and Mass Transfer 52 (2009) 5990–5999

Contents lists available at ScienceDirect

International Journal of Heat and Mass Transfer

journal homepage: www.elsevier.com/locate/ijhmt

Cooling transients in a sudden-expansion channel with varied rates of wall transpiration

Go-Long Tsai [a], Y.C. Lin [b], H.W. Wang [c], Y.F. Lin [c], Y.C. Su [c], J.T. Yang [b,*]

[a] Department of Vehicle Engineering, National Taipei University of Technology, Taipei 10608, Taiwan
[b] Department of Mechanical Engineering, National Taiwan University, Taipei 10617, Taiwan
[c] Department of Power Mechanical Engineering, National Tsing Hua University, Hsinchu 30013, Taiwan

ARTICLE INFO

Article history:
Received in revised form 7 August 2009
Available online 10 September 2009

Keywords:
Backstep
Sudden-expansion channel
Transpiration cooling

ABSTRACT

The transient cooling process in a sudden-expansion channel with the injection of cold air from the porous bottom wall is investigated experimentally. Four cooling patterns are categorized based on the structure of the corner eddy and the recirculation zone. Two mechanisms, porous-wall cooling and film cooling, are proposed to interpret the transition of the cooling patterns as the rate of wall injection is increased. At the early phase of wall injection, both the reattachment effect and the increased coolant injection induced by the low-pressure center are considered to produce the two maxima in spatial distributions of the Stanton number.

1. Introduction

Due to its frequent presence in engineering applications, the separation-reattachment flow within a sudden-expansion channel has been investigated extensively for decades (Eaton and Johnson [1]; Armaly et al. [2]; Shih and Ho [3]; Boizumault et al. [4]; and Tihon et al. [5]). Various flow patterns are involved, including corner eddy, recirculation vortex, shear layer, reattachment zone, and re-developing boundary layer. By incorporating additional fluid transpiration from the bottom wall downstream the backstep, the flow may either simulate the pyrolysis of solid fuel in an axial dump combustor (Richarson et al. [6]; Yang and Wu [7]), or serve as an efficient cooling approach that protects the wall from the hot inlet stream. The injected flow not only carries positive momentum into the reverse stream of the recirculation vortex, but also induces a favorable pressure gradient to counteract the adverse one downstream the backstep. Complicated transformations of the thermal flow patterns are introduced by the interactions between the inlet stream and the wall injection, which are worth thorough investigations.

Comprehensive research on the transpiration cooling has been conducted since 1990. Eckert and Cho [8] found that the Stanton number and the transpiration rate (the ratio of the injection velocity to the inlet velocity) were the dominant indices. On the other hand, the flow structure was observed to alter on increasing the fluid injection from the bottom wall. Collier and Schetz [9] indicated that the turbulence intensity and the Reynolds stress in the turbulent boundary layer were enhanced, while Cheng et al. [10] claimed that the pressure loss and the friction coefficient were both enlarged, though the heat transfer at the bottom wall was decreased. Similarly, the influence of the wall injection (with transpiration rates of 0–2%) upon the turbulence intensity, the characteristics of the boundary layer, and the friction coefficient of the wall was investigated by Rodet et al. [11]. Furthermore, four distinct flow patterns were categorized by Yang et al. [12] by increasing the wall injection velocity ratio gradually.

As far as the mechanisms of transpiration cooling are concerned, they may only be clarified via the analysis of the transient process from the perspectives of corresponding flow structures and patterns of heat transfer downstream the backstep. The characteristics of heat transfer and the shifting of the reattachment point were experimentally investigated by Tsou et al. [13]. The position at which the largest heat transfer coefficient occurred was found to be near the reattachment point, and a similar topic was numerically studied by Hsu et al. [14]. By introducing topology and numerical methods, Chiang et al. [15] also derived the transient transformation of the recirculation structure outside the main recirculation region. On the other hand, an experimental approach dedicated to the analysis of the transient transpiration cooling within a sudden-expansion channel was established by Yang et al. [16,17].

Although much progress in the understanding of heat and mass transfer within a sudden-expansion channel has been achieved, the intricate interactions and the mechanisms of mixing between the transpired fluid and the inlet stream necessitate further clarifications. In the present work, we explored the transient phenomena of heat and mass mixing in a sudden-expansion channel with

* Corresponding author.
E-mail address: jtyang@ntu.edu.tw (J.T. Yang).

0017-9310/$ - see front matter © 2009 Elsevier Ltd. All rights reserved.
doi:10.1016/j.ijheatmasstransfer.2009.08.006

Nomenclature

A_{in}	cross-sectional area of the inlet channel
A_w	area of the porous bottom wall
B	volume of the control volume
b	streamwise length of the control volume
C_p	specific heat under constant pressure of the wall-injected air
H	step height
L_T	dimensionless temperature level
$M_{s,mass}$	mass ratio per unit area
Nu	Nusselt number
Pr	Prandtl number
Q_{in}	volume flow rate of the inlet air stream
Q_w	volume flow rate of the injected air
q_{cv}	heat convection from the inlet stream
q_f	heat carried by the wall injection flow
q_l	heat conduction from the left
q_r	heat conduction from the right
q_w	heat conduction along the wall-normal direction
Re	Reynolds number
$S_{\triangle T}$	dimensionless rate of temperature decay
St	Stanton number
s	thickness of the porous bottom wall
T	temperature
T_{in}	temperature of the inlet air stream
T_w	temperature of the injected air
t	time
t^*	dimensionless time
u_{in}	velocity of the inlet air stream
v_w	mean superficial velocity of wall injection
X_r	reattachment length

Greek symbols

ρ_{in}	density of the inlet air stream
ρ_w	density of the injected air
Φ	porosity

varied rates of wall transpiration. With respect to the various wall injection rates, four patterns are identified based on the respective flow structures and thermal patterns, while two distinct mechanisms are proposed to dominate the transient cooling process.

2. Experiment design

A schematic diagram of the experiment setup is demonstrated in Fig. 1. The wind-tunnel system consists of an air blower (11.25 kW), a heating section, a test section, and systems for flow visualization, velocity diagnostics, and temperature measurement. The test section is a sudden-expansion channel (Fig. 2) with the height of the backstep H = 13 mm. The corresponding aspect ratio (the ratio of channel width to step height) is 15.4. Accordingly, the average flow downstream the backstep in the spanwise centerline plane is expected to be two-dimensional [18]. A porous sheet (width 200 mm × length 300 mm × thickness s 1.56 mm, porosity Φ = 40.8%) is installed as the bottom wall downstream the backstep. Note that since the thickness of the sheet is relatively insignificant comparing to the two other dimensions, the porosity is also treated as the ratio of the total pore area to the area of the bottom wall. A high-pressure chamber sustained at 7 bar is connected underneath to inject the low temperature air (T_w = 15 °C) through the porous sheet into the test section for the tests of transpiration cooling.

In this study, the heated inlet stream is maintained at 3.8 m/s (u_{in}), and the volume flow rates of the injected air (coolant) are varied from 0.833×10^{-3} to 5.0×10^{-3} m^3/s. The experiment matrix based on the main controlling variables of the inlet stream temperature T_{in} and the mean superficial velocity of wall injection v_w is demonstrated in Table 1. Note that the latter variable v_w is defined as the mean flow velocity at the pore exit of the porous bottom

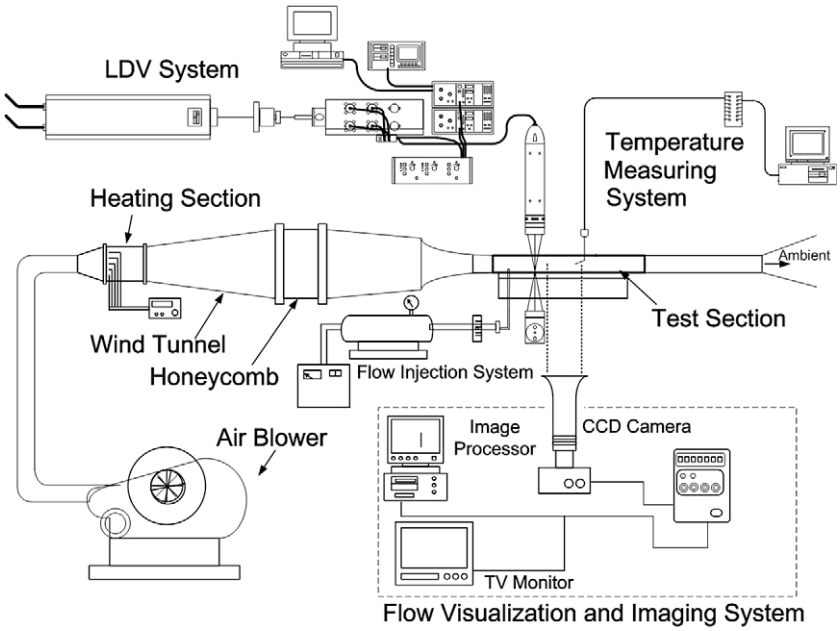

Fig. 1. Schematic diagram of the experiment setup.

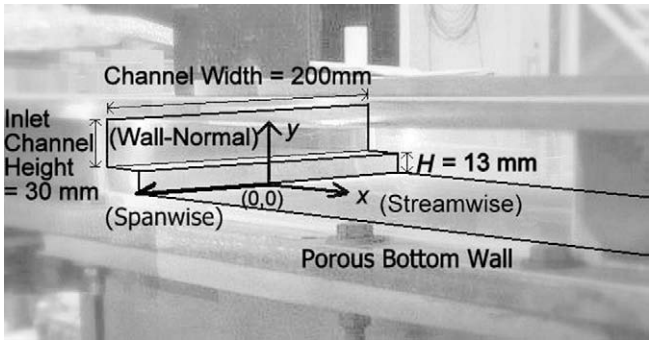

Fig. 2. Schematic drawing of the test section.

wall. To categorize the patterns and expand the applicability of the analysis [19], the mass ratio per unit area $M_{s,mass}$ is introduced, which is defined as

$$M_{s,mass} = \frac{\rho_w Q_w/\phi A_w}{\rho_{in} Q_{in}/A_{in}} = \frac{\rho_w v_w}{\rho_{in} u_{in}} \quad (1)$$

Accordingly, various patterns are categorized with respect to $M_{s,mass}$ based on the flow structures and the characteristics of cooling.

To facilitate the visualization of flow patterns, a laser sheet (thickness 1 mm) from an argon-ion laser (5 W) is established in combination with syringe-injected $TiCl_4$ particles, which generate hydrogen chloride (HCl) droplets on reacting with water vapor. The images are then recorded by a high-speed motion analyzer (Kodak KTAPRO-TM). The same argon-ion laser is also utilized as

Table 1
Experiment matrix and the corresponding pattern classification. u_{in} = 3.8 m/s, A_{in} = 0.006 m^2, ρ_w = 1.225 kg/m^3, T_w = 15 °C, A_w = 0.06 m^2.

u_{in} = 3.8 m/s, A_{in} = 0.006 m^2, ρ_w = 1.225 kg/m^3, T_w = 15 ℃ , A_w = 0.06 m^2												
	Q_w /10^{-3} m^{3}s^{-1}	0.833	1.250	**1.667**	2.083	**2.500**	2.916	3.333	3.750	**4.167**	4.583	5.000
	v_w /ms^{-1}	0.034	0.051	**0.068**	0.085	**0.102**	0.119	0.136	0.153	**0.170**	0.187	0.204
ρ_{in} /kgm^{-3}	T_{in} /℃	mass ratio per unit area $M_{s,mass}$										
1.185	25	0.009	0.014	0.018	0.023	0.027	0.032	0.036	0.041	0.046	0.050	0.055
1.093	50	0.010	0.015	0.020	0.025	0.03 0	0.035	0.040	0.045	0.050	0.055	0.059
1.014	75	0.011	0.016	0.021	0.027	0.032	0.037	0.043	0.048	0.053	0.059	0.064
0.947	100	0.011	0.017	0.023	0.029	0.034	0.040	0.046	0.052	0.057	0.063	0.069
0.887	***125***	0.012	0.018	***0.024***	0.031	***0.037***	0.043	0.049	0.055	***0.061***	0.067	0.073
0.835	150	0.013	0.019	0.026	0.032	0.039	0.045	0.052	0.058	0.065	0.073	0.078
0.788	175	0.014	0.021	0.027	0.034	0.041	0.048	0.055	0.062	0.069	0.076	0.082
0.746	200	0.015	0.022	0.029	0.036	0.044	0.051	0.058	0.065	0.073	0.080	0.087
0.709	225	0.015	0.023	0.031	0.038	0.046	0.053	0.061	0.069	0.076	0.084	0.092

T_{in} /℃ \ Q_w /10^{-3} m^{3}s^{-1}	0.833	1.250	1.667	2.083	2.500	2.916	3.333	3.750	4.167	4.583	5.000
25	recirculation pattern				elevated recirculation pattern			transpiration pattern			
50											
75											
100											
125											
150										film pattern	
175											
200											
225											

the light source of the two-component forward-scattered laser-Doppler velocimetry (LDV), from which the averaged velocity field is obtained. The aluminum oxide (Al_2O_3) powder is seeded into the flow when conducting LDV diagnostics. Further details about the LDV measurement, including its uncertainty analysis, are available in [12]. Total 40 thermocouples (K-type, 125 μm) are attached to 20 stages at both sides of the porous sheet to measure the temperature of the bottom wall, while the flow temperature is accessed via a tiny probe installed with another thermocouple (K-type, 25 μm). To map the spatial and temporal distributions of flow temperature, the probe is positioned at 224 locations (16 streamwise grids × 14 wall-normal grids) along the spanwise centerline plane via a two-axis positioning platform.

The uncertainty analysis for the temperature measurement is conducted at four locations: $(x, y) = (50\text{ mm}, 20\text{ mm})$, $(150\text{ mm}, 20\text{ mm})$, $(40\text{ mm}, 3\text{ mm})$, and $(90\text{ mm}, 3\text{ mm})$, for which $(x, y) = (0, 0)$ is the root of the backstep. Whereas the former two points are located in regions of little disturbance, the flow disturbances at the latter two locations are intense. Sixty sets of data, each comprising 1024 points, are adopted for pooled statistics of the temperature at each location. Based on 95% confidence level, the uncertainties are estimated to be 3.2–5.8% for the flow temperature and 2.2–4.8% for the wall temperature.

3. Results and discussion

3.1. The pattern classification via flow visualization and LDV diagnostics

Under the experiment setting of this study, it takes about one hour for the heated inlet stream to attain the prescribed temperature T_{in} while it is continuingly fed into the test section. After the

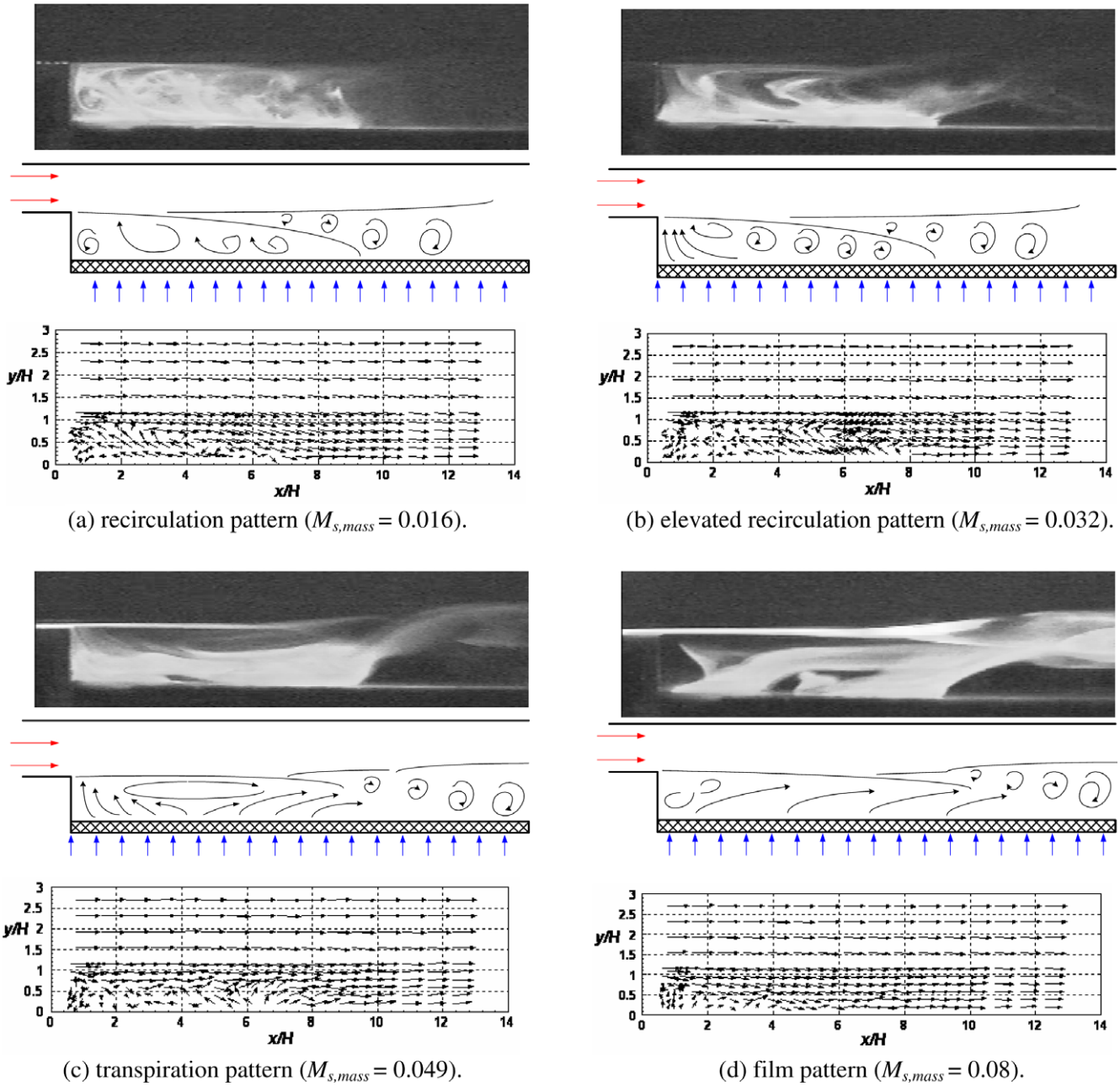

(a) recirculation pattern ($M_{s,mass} = 0.016$).

(b) elevated recirculation pattern ($M_{s,mass} = 0.032$).

(c) transpiration pattern ($M_{s,mass} = 0.049$).

(d) film pattern ($M_{s,mass} = 0.08$).

Fig. 3. Flow structures and the distributions of velocity vectors for the four flow patterns.

prescribed T_{in} is reached, the coolant (air; T_w = 15 °C) is injected from the porous bottom wall at t = 0. The flow is observed to reach a steady state 3 s after coolant injection [20]. Based on the distinct flow structures, four patterns are categorized with respect to $M_{s,mass}$: the recirculation pattern, the elevated recirculation pattern, the transpiration pattern, and the film pattern (Fig. 3). Besides the images and the schematic drawings of the flow structures based on the data from flow visualization, the distributions of velocity vectors obtained from the LDV diagnostics are demonstrated as well. The reattachment length (X_r) is about 70 mm (5–6 H) for the recirculation pattern (Fig. 3(a)). One of each two successive shedding vortices first turns downward to strike the bottom wall and then moves downstream. Part of the fluids carried by the reattached vortex moves upstream and joins the main recirculation bubble. The frequency of vortex shedding is observed to be around 20 Hz.

As the main recirculation bubble is slightly lifted by wall injection, the reattachment length X_r is greater (7.7 H) for the elevated recirculation pattern (Fig. 3(b)). Although the fluids near the wall still move either upstream or downstream, the impinging effect of the vortex is weaker than that of the recirculation pattern. Increasing the wall injection transforms the flow into the transpiration pattern (Fig. 3(c); the X_r is about 10 H). The adverse pressure gradient is almost diminished due to the enormous coolant injected. Further increasing the wall injection results in the flow feature identified as the film pattern (Fig. 3(d)). No noticeable reattachment of the flow is observed and the main recirculation vortex is completely destroyed. Most of the mixing between the heated inlet stream and the injected coolant occurs at the horizontal planar shear layer, except for the flow neighboring the backstep.

Distinct flow structures at the corner of the backstep are also observed. A second flow separation, which produces the corner

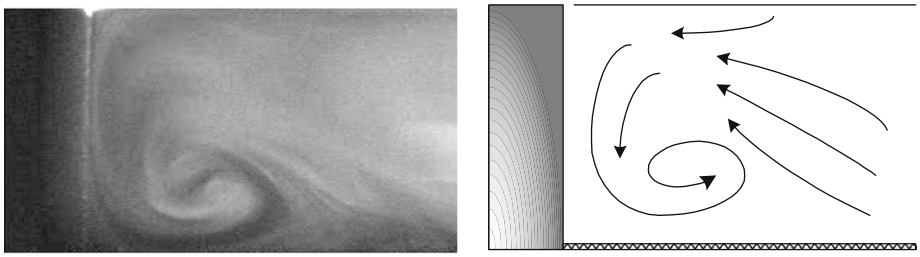

(a) recirculation pattern ($M_{s,mass}$ = 0.016).

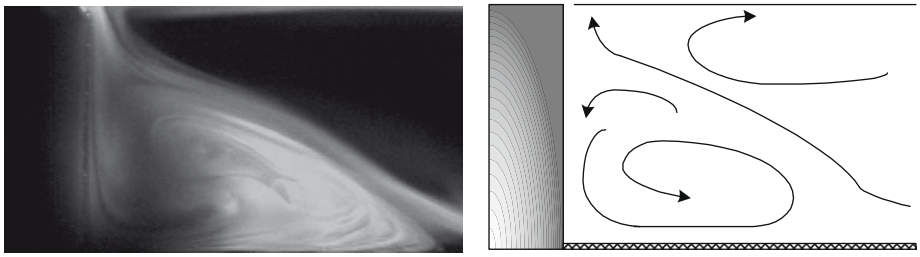

(b) elevated recirculation pattern ($M_{s,mass}$ = 0.032).

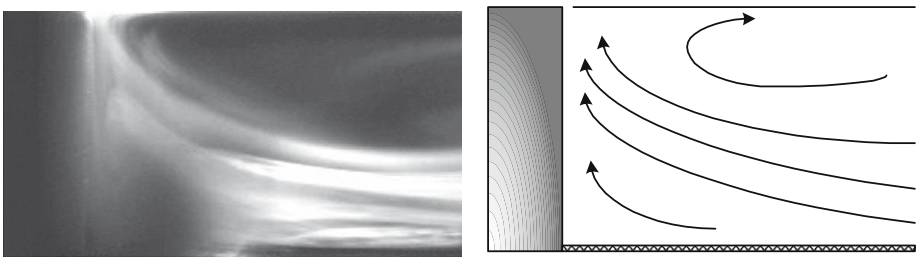

(c) transpiration pattern ($M_{s,mass}$ = 0.049).

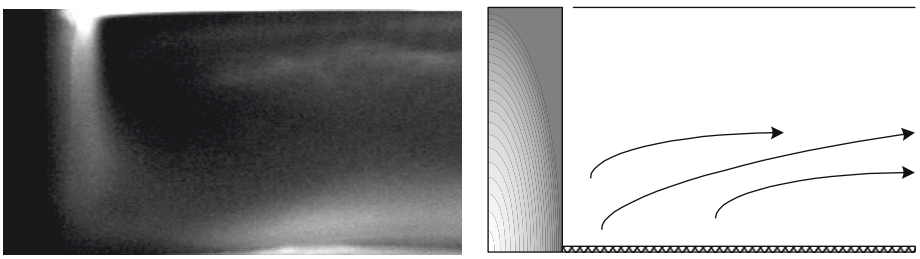

(d) film pattern ($M_{s,mass}$ = 0.08).

Fig. 4. Flow structure near the corner of the backstep for the four flow patterns.

eddy, is introduced due to the momentum carried by the recirculation of flow. A corner eddy with a streamwise length of 1 H is found to oscillate at 2.5 Hz for the recirculation pattern (Fig. 4(a)). As more coolant is injected for the elevated recirculation pattern, the fluids in the corner are further blocked from flowing downstream, which produces a larger corner eddy (Fig. 4(b)). Nonetheless, intermittent release of the fluids accumulated within the corner eddy into the main recirculation bubble is observed. Although complicated interactions between the flow in the step corner and the lifted recirculation bubble are revealed, there is no significant corner eddy structure for the transpiration flow pattern (Fig. 4(c)). In contrast, a corner eddy is barely sustained for the film pattern, within which the fluids in the corner move directly downstream (Fig. 4(d)).

Accordingly, the experiment conditions in Table 1 are reorganized based on their respective patterns, as indicated in the table itself and Fig. 5. Note that the four patterns correspond respectively to patterns A, B, C, and D in [12], in which detailed analyses of the flow structures are demonstrated.

3.2. Spatial and temporal distributions of the flow temperature

To analyze the characteristics of cooling for the various patterns, a specified inlet stream (u_{in} = 3.8 m/s, T_{in} = 125 °C) with three specific rates of injection (1.667×10^{-3}, 2.5×10^{-3} and 4.167×10^{-3} m^3/s) are analyzed in detail. The corresponding $M_{s,mass}$ are 0.024 (recirculation pattern), 0.037 (elevated recirculation pattern), and 0.061 (transpiration pattern), respectively. The film

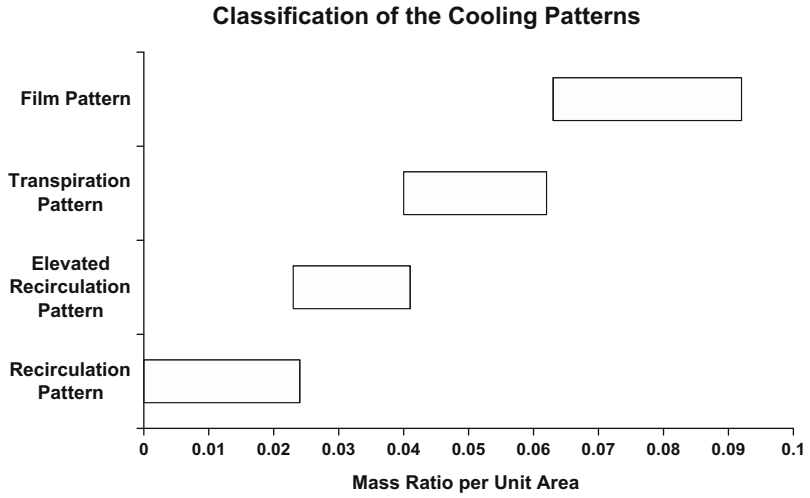

Fig. 5. Classification of the cooling patterns with respect to the mass ratio per unit area $M_{s,mass}$.

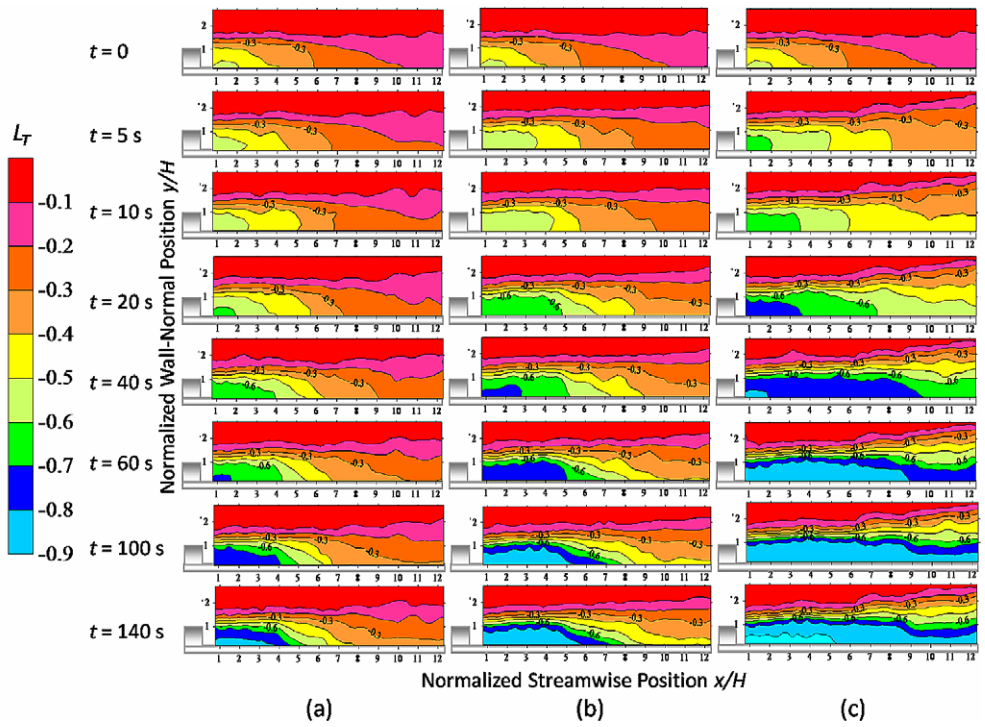

Fig. 6. Spatial and temporal L_T distributions of the flow: (a) recirculation pattern ($M_{s,mass}$ = 0.024); (b) elevated recirculation pattern ($M_{s,mass}$ = 0.037) and (c) transpiration pattern ($M_{s,mass}$ = 0.061).

pattern is not addressed here since it is essentially an evolvement of the transpiration pattern. To evaluate the effectiveness of cooling for each flow pattern, we analyze the spatial and temporal distributions of the flow temperature via a dimensionless temperature level, L_T, which is defined as

$$L_T = \frac{T - T_{in}}{T_{in} - T_w} \tag{2}$$

in which T, T_{in} and T_w denote the temperatures of the flow, the inlet stream, and the injected coolant, respectively.

In this study, the thermal field is observed to reach a steady state 140 s after coolant injection. Accordingly, the distributions of L_T from the time of coolant injection ($t = 0$) to $t = 140$ s for the recirculation pattern, the elevated recirculation pattern, and the transpiration pattern, are demonstrated in Fig. 6. For the recirculation pattern ($M_{s,mass} = 0.024$, Fig. 6(a)), the region of low temperature appears near the step corner prior to coolant injection, and it extends downstream thereafter. A cooled zone with $L_T < -0.8$ appears at $t = 60$ s, and a region with intensive cooling is found to evolve upstream. At $t = 140$ s, the L_T distributions become steady and the cooled region with $L_T < -0.8$ is located upstream $x = 5\ H$ and below $y = 0.7\ H$.

The low temperature zone for the elevated recirculation pattern ($M_{s,mass} = 0.037$, Fig. 6(b)) is broader and develops more rapidly than that of the recirculation pattern. The cooled region with $L_T < -0.8$ covers the region upstream $x = 7\ H$ and below $y = 0.8\ H$. The cooling tendency for the transpiration cooling pattern ($M_{s,mass} = 0.061$, Fig. 6(c)) is similar to those of the previous two patterns; the cooled region with $L_T < -0.8$ spreads over the entire bottom wall surface at $t = 60$ s and finally attains a steady state at $t = 140$ s.

To evaluate the rate of cooling within the flow, a dimensionless rate of temperature decay $S_{\triangle T}$ is introduced, which is defined as

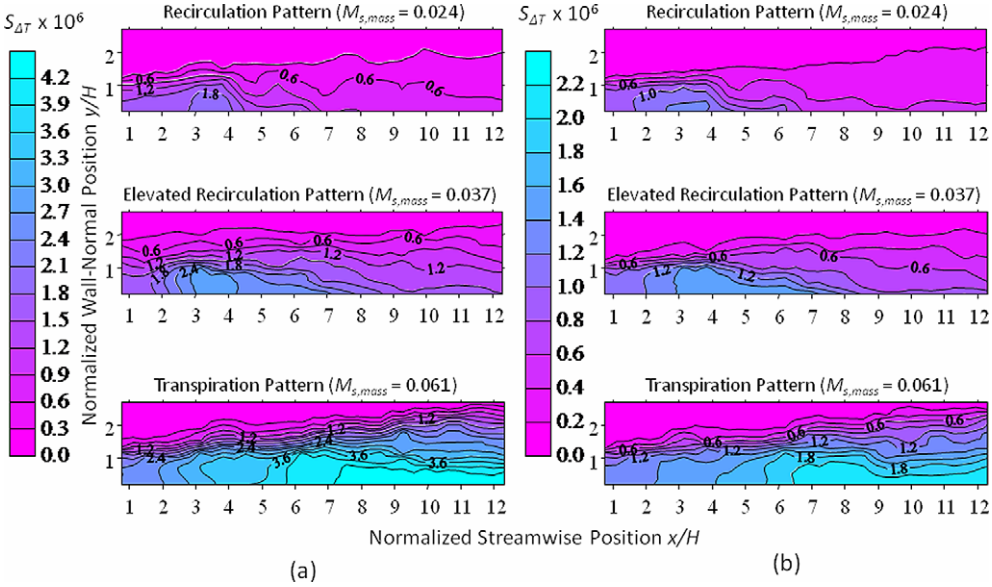

Fig. 7. Temporal evolution of the $S_{\triangle T}$ distribution for various cooling patterns; (a) $t = 60$ s and (b) $t = 140$ s.

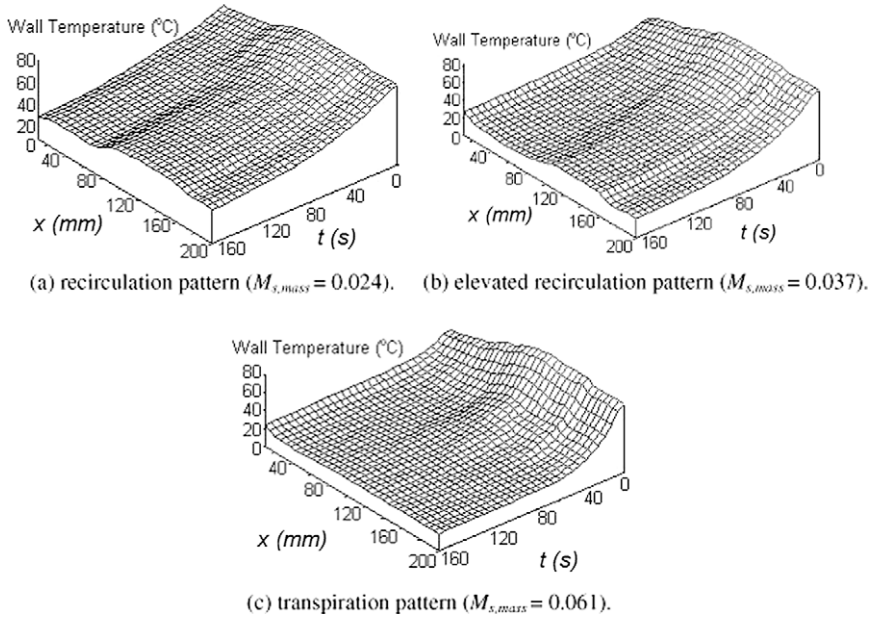

Fig. 8. Spatial and temporal distributions of the temperature at the bottom wall surface.

$$S_{\Delta T} = \frac{(L_T)_{t_1} - (L_T)_{t_2}}{\Delta t^*} \tag{3}$$

in which t_1 and t_2 denote two instants and t^* (the dimensionless time) is defined as

$$\Delta t^* = \frac{u_{in}(t_2 - t_1)}{H} \tag{4}$$

A larger $S_{\triangle T}$ indicates a greater rate of temperature decay.

Fig. 7 demonstrates the distributions of $S_{\triangle T}$ at $t = 60$ s and $t = 140$ s ($t = 60$ s and $t = 140$ s respectively for t_2 with $t = 0$ for t_1). The region with the largest $S_{\triangle T}$ gradually extends downstream when the cooling pattern is transformed from recirculation to transpiration. The region with the largest $S_{\triangle T}$ in the recirculation cooling pattern ($M_{s,mass} = 0.024$) locates at $x = 3$–$4\,H$ near the wall, which is also the contact zone between the accumulated coolant near the corner eddy and the recirculating heated inlet stream near the reattachment region.

For the elevated recirculation pattern ($M_{s,mass} = 0.037$), the largest $S_{\triangle T}$ occurs at $x = 3$–$6\,H$. The increased wall injection broadens the mixing region between the heated inlet stream and coolant, which produces a broader region with large $S_{\triangle T}$. On the contrary, a cooled layer is observed to develop downstream the reattachment zone in the transpiration pattern ($M_{s,mass} = 0.06$). The specific phenomenon is illustrated here as the film-cooling mechanism. Consequently, in addition to the large $S_{\triangle T}$ zone within the recirculation bubble, another intensive mixing zone with large $S_{\triangle T}$ is observed to locate downstream $x = 6\,H$ at $t = 60$ s, as depicted in Fig 7(a). Fig. 7(b) further shows that, for the transpiration pattern, the whole region with large $S_{\triangle T}$ is dominated by the cooled layer (or film-cooling mechanism) at $t = 140$ s, whereas the cooling characteristics of the previous two patterns at $t = 140$ s remain similar to those at $t = 60$ s.

3.3. Spatial and temporal temperature distributions at the bottom wall surface

The spatial and temporal temperature distributions at the bottom wall surface for the three patterns are exhibited in Fig. 8. Generally, the section with lower temperature first appears around the recirculation bubble, and then the temperature of the whole bottom wall is gradually decreased to a similar level. Nonetheless, the distinction between the wall temperature within the recirculation zone and the re-developing region is disappeared as the cooling pattern transforms from elevated recirculation to transpiration. This similar feature is also revealed by the temperature level L_T of the flow (Fig. 6). The phenomenon implies that the cooling is controlled by mechanisms varying as the transition of the flow patterns proceeds. While the cooling is considered to be dominated by the main recirculation bubble (described here as the porous-wall cooling mechanism) for the recirculation pattern, the film-cooling mechanism is perceived to be dominant for the transpiration pattern.

The temporal L_T evolutions at the bottom wall surface for the three investigated patterns are shown in Fig. 9. Since the entire recirculation region is at a lower temperature, the L_T downstream $x = 7H$ is invariably larger than that upstream. A significant decrease of temperature is achieved during the interval $t = 10$–70 s for all three patterns, whereas the largest temperature decay occurs before $t = 20$ s. Although the flow pattern becomes steady 3 s after coolant injection according to the data from flow visualization, more than 120 s are required for the temperature at the porous wall surface to attain a steady state. Correspondingly, the distributions of the flow temperature attain a steady condition 140 s after coolant injection.

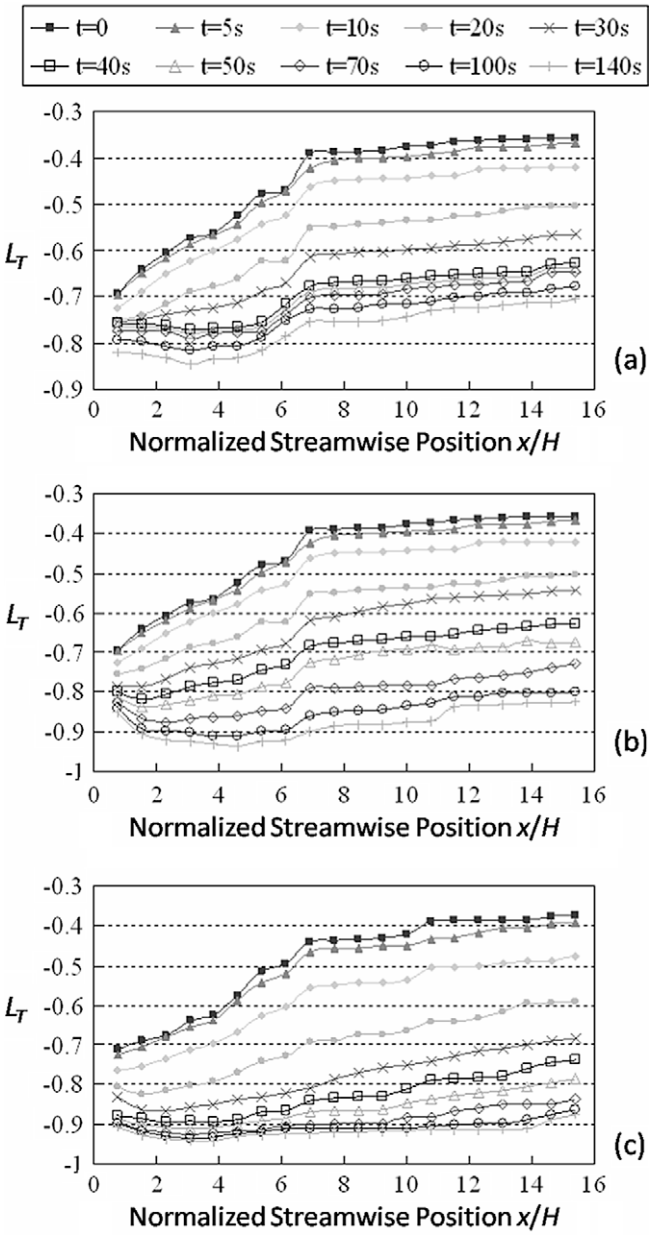

Fig. 9. Temporal evolution of the L_T at the bottom wall surface; (a) recirculation pattern ($M_{s,mass} = 0.024$); (b) elevated recirculation pattern ($M_{s,mass} = 0.037$) and (c) transpiration pattern ($M_{s,mass} = 0.061$).

3.4. Heat transfer analysis at the bottom wall

The control volume for a heat-flux analysis of the porous bottom wall is depicted in Fig. 10. An equation for conservation of energy (neglecting radiation) is

$$q_l + q_r + q_{cv} - q_w - q_f = \rho w B C_p \frac{\partial T}{\partial t} \tag{5}$$

in which B denotes the volume of the control volume with unit depth and equals to $b \times s$. Based on the temperature diagnostics within the porous bottom wall, of which 40 thermocouples are attached to both sides, the respective magnitude of q_l, q_r, and q_f is evaluated to be less than 5% of the total heat transfer [20–22]. Accordingly, the equation is simplified to

$$q_{cv} = q_w + \rho w B C_p \frac{\partial T}{\partial t} \tag{6}$$

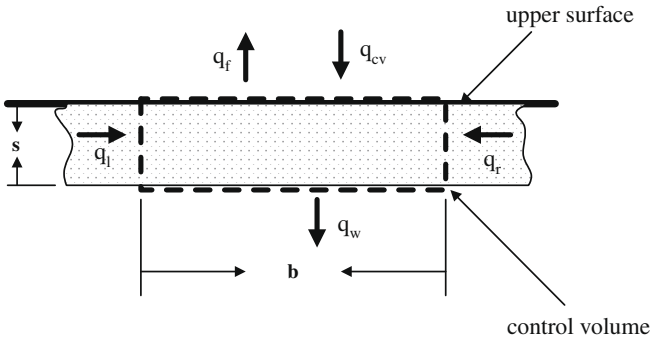

Fig. 10. Schematic diagram of the control volume for heat-transfer analysis.

and the Stanton number is defined as

$$St = \frac{Nu}{RePr} = \frac{q_{cv}}{\rho w u_{in} C_p \Delta T b} \tag{7}$$

The spatial and temporal distributions of the Stanton number for the investigated cooling patterns are shown in Fig. 11. Two maxima of the Stanton number occur at the beginning of the coolant injection; one is near the step corner, and the other locates at the reattachment zone. The former is attributed to the greater coolant injection induced by the low pressure (the low-pressure center locates at x = 2.5–3.5 H) [12]. Accordingly, the temperature difference across the porous sheet is increased. Nonetheless, since the convective heat transfer is diminished as the flow achieves a steady state, the temperature difference across the bottom wall near the step corner is decayed rapidly and this maximum quickly disappears.

The other maximum of the Stanton number that occurs in the reattachment zone is attributed to the impinging of the heated inlet stream on the bottom wall, which introduces intense convective heat transfer. As the coolant injection proceeds, a low-temperature layer of fluids is formed adjacent to the porous sheet. The thickness of the layer is gradually increased, and the temperature difference between the heated fluids above the wall surface and the wall itself is decreased. Accordingly, the convective heat transfer is diminished, and the Stanton number is decreased as well. This maximum is decreased much slower than the previous one due to the continuing impingement of the heated inlet stream. On the other hand, as the shedding vortices along the shear layer intermittently strike the bottom wall at about 23 Hz, the cooling effectiveness is relatively insignificant near the reattachment point.

The temporal evolutions of the Stanton number for the cooling patterns during the initial phase of cooling also provide some insights into the characteristics of heat transfer. Comparing to the two other patterns, the dominance of film-cooling for the transpiration pattern is evidenced by the fact that the maximum of the Stanton number near the step corner is relatively insignificant. The dominance of porous-wall cooling, on the other hand, is demonstrated via the significant decrease of the Stanton number near the step corner for the recirculation and elevated recirculation patterns.

4. Conclusions

The transient processes of heat transfer between the heated inlet stream and the coolant injected from the bottom wall within a sudden-expansion channel are experimentally investigated. Under various rates of coolant injection, distinct flow features are identified based on both LDV diagnostics and flow visualization of the recirculation bubble and the corner eddy. Four cooling patterns – the recirculation pattern, the elevated recirculation pattern, the

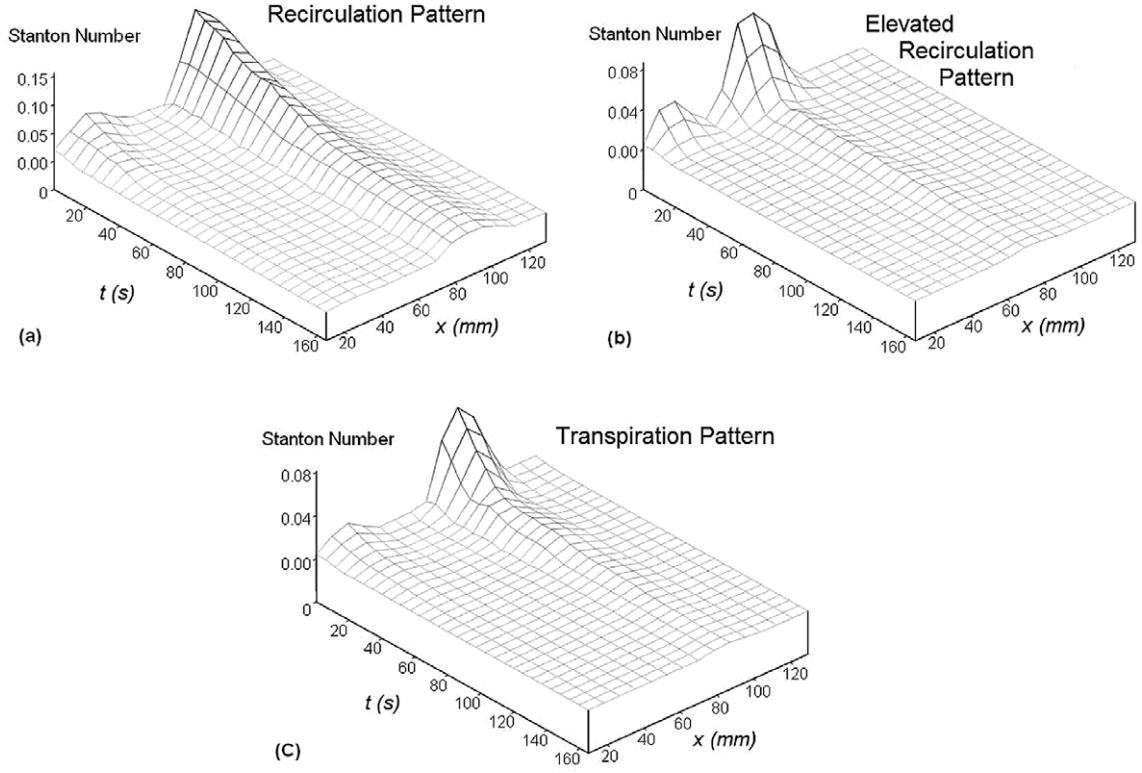

Fig. 11. Spatial and temporal distributions of the Stanton number: (a) recirculation pattern ($M_{s,mass}$ = 0.024); (b) elevated recirculation pattern ($M_{s,mass}$ = 0.037) and (c) transpiration pattern ($M_{s,mass}$ = 0.061).

transpiration pattern, and the film pattern – are recognized. Measurements of both flow and wall temperatures reveal distinct characteristics of cooling, and the dominant mechanisms are proposed accordingly.

For the recirculation pattern, the reattachment point locates at $x = 5–6\ H$. The structure of the corner eddy is evident, which oscillates at 2.5 Hz. The region with the lowest temperature appears first in the corner vortex and then extends downstream. On the other hand, the region with the greatest rate of temperature decay locates at the middle section of the recirculation region. Intensive cooling is initiated at $t = 60$ s and the cooled zone is limited to be upstream the reattachment region. For the elevated recirculation pattern, the reattachment length X_r is increased (7.7 H) comparing to the recirculation pattern. Periodic oscillations of the corner eddy are insignificant. Although the region with the lowest temperature is similar to that of the recirculation pattern, the zone of intensive cooling is broader and appears earlier at $t = 40$ s. For the transpiration pattern, the adverse pressure gradient is no longer sustained, and the recirculation bubble is noticeably lifted and squeezed. The cooling region is much wider and eventually covers the entire bottom wall surface. On the other hand, intensive cooling is first introduced as early as $t = 20$ s. The detailed investigation performed in this work clarifies that the distinctions between the recirculation and transpiration patterns are attributed to the transition of the dominant mechanisms. The recirculation pattern is dominated by the recirculation vortex, or the porous-wall cooling mechanism, whereas the transpiration pattern is completely controlled by the film-cooling mechanism.

During the initial phase of coolant injection, there are two maxima in the spatial distributions of the Stanton number. One occurs near the step corner due to the greater wall injection induced by the low pressure there. The other that locates at the reattachment region is introduced by the impingement of the shedding vortices. As the wall injection continues, the porous-wall cooling mechanism near the step corner is effectuated, and that maximum disappears rapidly. The other maximum is kept in the reattachment region, which is decayed subsequently.

Acknowledgement

This work is supported by the National Science Council of the Republic of China (Taiwan) under the contract NSC-91-2212-E-007-063.

References

[1] J.K. Eaton, J.P. Johnston, A review of research on subsonic turbulent flow reattachment, AIAA J. 19 (1981) 1093–1100.
[2] B.F. Armaly, F. Durst, J.C.F. Pereira, B. Schonung, Experimental and theoretical investigation of backward-facing step, J. Fluid Mech. 127 (1983) 473–496.
[3] C. Shih, C.M. Ho, Three-dimensional recirculation flow in a backward facing step, J. Fluids Eng. 116 (1994) 228–232.
[4] F. Boizumault, S. Harmand, B. Desmet, Influence of the characteristics of an aerodynamically perturbated flow on the local heat transfer by convection from a wall, Int. J. Heat Mass Transfer 43 (2000) 791–806.
[5] J. Tihon, J. Legrand, P. Legentilhomme, Near-wall investigation of backward-facing step flows, Exp. Fluids 31 (2001) 484–493.
[6] J. Richardson, W.A. de Groot, J.I. Jagoda, R.E. Waiterick, J.E. Hubbartt, E.C. Strahle, Solid fuel ramjet simulator results: experiment and analysis in cold flow, J. Propulsion Power 24 (1985) 1956–1963.
[7] J.T. Yang, C.Y.Y. Wu, Controlling mechanisms of ignition of solid fuel in a sudden-expansion combustor, J. Propulsion Power 11 (1995) 483–488.
[8] E.R.G. Eckert, H.H. Cho, Transition from transpiration to film cooling, Int. J. Heat Mass Transfer 37 (Suppl. 1) (1994) 3–8.
[9] F.S. Collier Jr., J.A. Schetz, Injection into a turbulent boundary layer through different porous surfaces, AIAA J. 22 (6) (1984) 839–841.
[10] Y.C. Cheng, G.J. Hwang, M.L. Ng, Developing laminar flow and heat transfer in a rectangular duct with one-walled injection and suction, Int. J. Heat Mass Transfer 37 (1994) 2601–2613.
[11] J.C. Rodet, G.A. Campolina-Franca, P. Pagnier, R. Morel, A. Lallemand, Experimental study of transpiration gas cooling through porous walls, Revue Generale de Thermique 37 (1997) 123–136.
[12] G.L. Tsai, Y.C. Lin, W.J. Ma, H.W. Wang, J.T. Yang, Transitional flow patterns behind a backstep with porous-based fluid injection, Int. J. Heat Mass Transfer 52 (2009) 1058–1069.
[13] F.K. Tsou, S.J. Chen, W. Aung, Starting flow and heat transfer downstream of a backward-facing step, J. Heat Transfer 113 (1991) 583–589.
[14] C.H. Hsu, Y.P. Chang, B.C. Chen, Transient mixed convection of a second-grade fluid past a backward-facing step, Int. Non-Linear Mech. 34 (1999) 881–893.
[15] T.P. Chiang, T.W.H. Sheu, C.C. Fang, Numerical investigation of vortical evolution in a backward-facing step expansion flow, Appl. Math. Model. 23 (1999) 915–932.
[16] J.T. Yang, J.D. Gu, W.J. Ma, Transient cooling effect by wall mass injection after backstep in high temperature flow field, Int. J. Heat Mass Transfer 44 (2001) 843–855.
[17] J. T. Yang, H. W. Wang, Y. F. Lin, Y. C. Su, Cooling transience in sudden-expansion channel with various wall transpiration rate, in: Proceedings of the 4th Pacific Symposium on Flow Visualization and Image Processing, Chamonix, France, 2003.
[18] V. de Brederode, P. Bradshaw, Three-dimensional flow in normally two-dimensional separation bubbles: I. Flow behind a backward-facing step, Aeronautical Report, Imperial College, 1972, pp. 72–191.
[19] H. W. Wang, Flow mixing and cooling mechanism in a transpirating sudden-expansion channel, Master thesis, National Tsing Hua University, Taiwan, 2002.
[20] Y. C. Su, Transient phenomena of transpiration cooling in high-temperature, Master thesis, National Tsing Hua University, Taiwan, 2001.
[21] J.T. Yang, C.H. Tsai, High temperature heat transfer of separated flow over a sudden-expansion with base mass injection, Int. J. Heat Mass Transfer 39 (1996) 2293–2301.
[22] W. J. Ma, Transpiration Cooling Phenomena in Separated-Flow Field, Ph.D. thesis, National Tsing Hua University, Taiwan, 2000.